Available online at www.sciencedirect.com

ScienceDirect

Procedia Structural Integrity 12 (2018) 448–456

Structural Integrity Procedia

www.elsevier.com/locate/procedia

AIAS 2018 International Conference on Stress Analysis

Structural validation of a realistic wing structure: the RIBES test article

Corrado Groth[a,*], Stefano Porziani[a], Andrea Chiappa[a], Francesco Giorgetti[a], Ubaldo Cella[a], Fabrizio Nicolosi[b], Pierluigi Della Vecchia[b], Franco Mastroddi[c], Giuliano Coppotelli[c], Marco Evangelos Biancolini[a]

[a] *University of Rome "Tor Vergata", 00133 Rome, Italy*
[b] *University of Naples "Federico II", 80125 Naples, Italy*
[c] *University of Rome "La Sapienza", 00184 Rome, Italy*

Abstract

Several experimental test cases are available in literature to study and validate fluid structure interaction methods. They, however, focus the attention mainly on replicating typical cruising aerodynamic conditions forcing the adoption of fully steel made models able to operate with the high loads generated in high speed facilities. This translates in a complete loss of similitude with typical realistic aeronautical wing structures configurations.

To reverse this trend, and to better study the aerolastic mechanism from a structural point of view, an aeroelastic measurement campaign was carried within the EU RIBES project. A half wing model for wind tunnel tests was designed and manufactured replicating a typical metallic wing box structure, producing a database of loads, pressure, stress and deformation measurements.

In this paper the design, manufacturing and validation activities performed within the RIBES project are described, with a focus on the structural behavior of the test article. All experimental data and numerical models are made freely available to the scientific community.

Keywords: FSI; Experimental Validation; Structural Validation; CFD; CSM

1. Introduction

Verification and validation is an essential mean to evaluate performance and reliability of computational tools. By assessing how accurately computational results compare with experimental data it is possible to investigate not only the accuracy but also the limits of the models, making experimental campaigns fundamentals to attest the trustworthiness of the tools in a modeling-and-simulation-based design scenario. While engineers are nowadays confident on the

* Corresponding author. Tel.: +39-06-7259-7143
E-mail address: Corrado.groth@uniroma2.it

10.1016/j.prostr.2018.11.073

range of applicability of commercial Computational Fluid Dynamic (CFD) and Computational Structural Mechanics (CSM) software, being them already extensively tested and validated, they still struggle to find a proper validation for Fluid Structure Interaction (FSI) methods in which those CFD and CSM solvers are coupled. For this reason in literature several experimental static and dynamic aeroelastic test cases are available, such as the AGARD 445.6 (Yates (1988)), HiReNASD (Chwalowski et al. (2011)) and ASDMAD (Chen et al. (2010)) between others. Since these projects focus however on replicating typical cruising aerodynamic conditions, involving huge loads typical of high speed facilities, structural models are generally made of full steel, losing any similitude to the tipical structural topologies employed in aeronautical construction.

To fill this gap, and to better study the aeroelastic mechanism from a structural point of view, an experimental campaign was carried within the EU RIBES project (European Commission (2018),Ribes (2018)). The "RIBES" (Radial basis functions at fluid Interface Boundaries to Envelope flow results for advanced Structural analysis) project, led by the University of Rome "Tor Vergata" in the framework of Clean Sky, was funded within the 7th European Union's Research and Innovation funding program and had a duration of two years. The aim of the RIBES project was focused on developing an innovative approach for loads mapping based on Radial Basis Functions (RBF) theory Biancolini (2012) and a suite of tools devoted to the improvement of accuracy in coupled FSI analyses. The research covered three main topics:

- Development of a load mapping procedure;
- Development of a structural optimization procedure;
- Setup of an experimental campaign.

While the outcomes from the first two topics have been previously disseminated in literature (Biancolini et al. (2018), Beltramme (2015), Cella et al. (2015)), this paper will be centered on the latter, for which a brand new test article had to be designed and manufactured. In the next sections the RIBES wing will be detailed, with a particular attention to the structural aspects of its design, testing and validation. First the topology and geometry of the RIBES wing will be explained, higlighting the methodologies employed and the design process. Then, since the subject of the paper is the structural validation activity, a brief overview into the experimental facility and testing will be given. To conclude the paper results and validation activities will be shown.

2. Experimental campaign requirements and wing design

The RIBES test case was built with the aim of being tested in a low speed wind tunnel in order to contain costs but, differently from the notables aeroelastic test cases previously cited, a realistic wing design was employed. A requirement for the test article design was indeed to replicate a typical wing box structure by recurring to all the traditional elements composing it such as spars, ribs and skin, but also to replicate a plausible real-life load distribution when tested at wind tunnel flow conditions, preferably an elliptical spanwise load shape. In order to fulfill these requirements the wing geometry and topology had to be designed to provide high deformations with moderate loads, but the adoption of a metal aeronautical structure and the scaling effects linked to the required wing span of 1.6 meters are conflicting targets. A simple scaling of an existing wing was unfeasible for manufacturing reasons, reducing skin thicknesses and rivets to unmanageable dimensions. This last aspect was crucial in designing a proper test article, since the greater complexity encountered was to be able to maximize deformations maintaining a wing topology with manageable and assemblable sheet plates, without sacrificing safety.

The final wing layout was reached after several iterations involving also model manufacturers, CFD and FEM simulations in the loop. While CFD analyses were important to set a target shape profile and were employed early in the design process, FEM simulations were crucial to assess the wing behavior, steering wing topology definition and dimensioning under stress and deformations objectives.

The final layout of the model, shown in figure 1, consists in a span of 1.6 m, root and tip chords of, respectively, 0.6 m and 0.42 m. The taper ratio of the resulting straight wing is 0.7. The wing profile, shown in figure 2, was obtained by scaling the original Göttingen 398 profile to a thickness $t/c = 11\%$ and by redesigning the leading edge to reduce and delay stall (Cella (2015)).

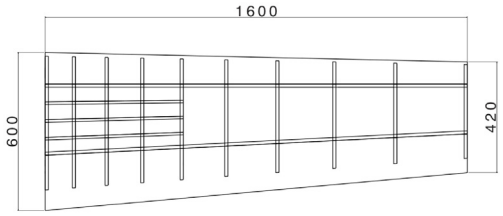

Fig. 1. RIBES wing layout and dimensions

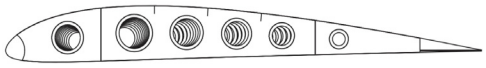

Fig. 2. RIBES wing airfoil profile

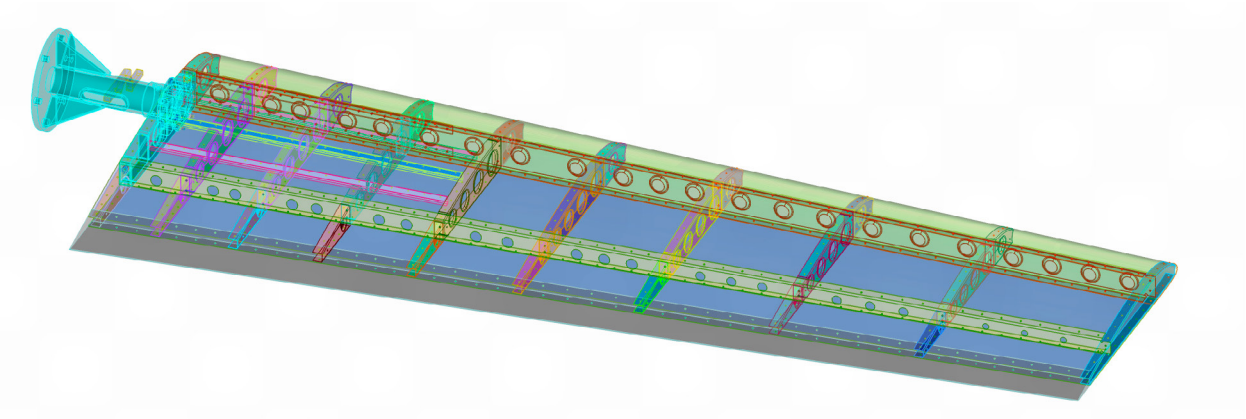

Fig. 3. RIBES wing CAD geometry

Wing topology consists in ten ribs and two C-shaped spars. Since no twist exists, spars are interested only by tapering and the front one is orthogonal to the root plane at a position of 20% of the root chord. Rear spar is located at 60% of the chord. Reference surface is 0.816 m^2. The CAD model of the full geometry is shown in figure 3.

FEM simulations during the preliminary design of the wing were of paramount importance, driving the choice of plate thicknesses and reinforcements in the areas of high stress. The most restrictive aspect during design process demonstrated to be the instability of compressed plates in the upper surfaces of the wing. By dimensioning the test article according to the nominal operative conditions of the wing tunnel, a 60 Kg of lift force was taken into account, originated by a 40 m/s wind velocity and validated by means of CFD simulations. This lift force, distributed elliptically as previously noticed, pushes upward the wing, that behaves as a cantilever beam with fixed root. Maximum moment is found at wing root, were pressure side plates are put under traction and suction side ones are compressed. While the requirement of high deformations with low wind speeds pushes toward a reduction of thicknesses, buckling instability become a problem that can be solved thickening the plates involved.

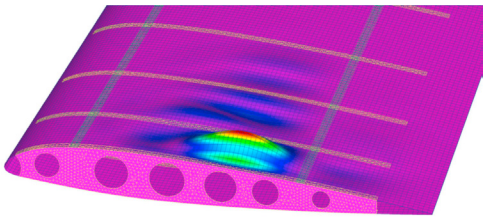

Fig. 4. Buckling of the root plates during preliminary design

This behavior was highlighted also in the preliminary FEM simulations in which local instabilities of the plates were encountered in the first bay as shown in figure 4. These preliminary studies drove design toward the use of stringers on the upper skin, applying three reinforcements covering the first four bay. Since the load is supported mainly by the skin, moreover, in case of a instability failure of upper plates, the spars wouldn't be dimensioned in order to support the structure. To provide enough margin of error, and to reduce the risk of damage to the structure, the front spar was thickened by applying 4 mm thick plates to the root area, where the stress is higher. Thicknesses and geometrical dimensions were chosen in order to assure a safety factor between 1.2 and 1.3.

Since 25 strain gauges and 81 pressure taps were planned to be installed, the wing skin was divided into four main sections providing enough space to the operator when mounting the sensors. Upper, lower, leading and trailing edge panels were attached to the structure by means of flush head CherryMAX rivets and subjected, as the other components, to Alodine treatment and primer for the paint. The strain gauges position on the model and their ID are shown in table 1.

Table 1. Strain gauges locations number, number and type

ID	Bay	POSITION	INSTALLATION	TYPE	y (mm)	eta
1	1	between rib1-rib2	front spar	UNIDIRECTIONAL	35.5	0.025
2	1	between rib1-rib2	front spar	UNIDIRECTIONAL	35.5	0.025
3	1	between rib1-rib2	rear spar	UNIDIRECTIONAL	35.5	0.025
4	1	between rib1-rib2	rear spar	UNIDIRECTIONAL	35.5	0.025
5	3	between rib3-rib4	front spar	UNIDIRECTIONAL	310	0.194
6	3	between rib3-rib4	front spar	UNIDIRECTIONAL	310	0.194
7	3	between rib3-rib4	rear spar	UNIDIRECTIONAL	297	0.194
8	3	between rib3-rib4	rear spar	UNIDIRECTIONAL	297	0.194
9	5	between rib5-rib6	front spar	UNIDIRECTIONAL	600	0.391
10	5	between rib5-rib6	front spar	UNIDIRECTIONAL	600	0.391
11	5	between rib5-rib6	rear spar	UNIDIRECTIONAL	598	0.391
12	5	between rib5-rib6	rear spar	UNIDIRECTIONAL	598	0.391
13	1	between rib1-rib2	front spar thickening	UNIDIRECTIONAL	35.5	0.025
14	1	between rib1-rib2	front spar thickening	UNIDIRECTIONAL	35.5	0.025
15	1	1stbay, between 1st and 2nd stringer	Upper Skin	UNIDIRECTIONAL	35.5	0.025
16	1	1stbay, correspondence to UD N.15	Lower Skin	ROSETTE-3SIGNAL	35.5	0.025
17	2	2ndbay, between 1st and 2nd stringer	Upper Skin	UNIDIRECTIONAL	169	0.106
18	2	2ndbay, between 2nd and 3rd stringer	Upper Skin	ROSETTE-3SIGNAL	169	0.106
19	1	between rib1-rib2	front spar	ROSETTE-3SIGNAL	35.5	0.025

3. Test facility and measurements

The measurement campaign involving the RIBES wing was hosted in the low speed wind tunnel of the University of Naples "Federico II". This facility is a closed circuit with a 2 meters wide test section and an airflow speed limit of 45 m/s. The balances measurement limits in this wind tunnel are 1000 N for the lift and 200 N for the drag, and the turbulence level is in the order of 0.1%. The model was installed on the side wall of the test section as a cantilever, as shown in figure 5.

The flow speed of measurements ranged between 30 and 40 m/s, for Mach numbers between 0.1 and 0.12 approximately. The obtained Reynold numbers ranged between 1 and 1.4 million taking into account a Mean Aerodynamic Chord (MAC) of 515 mm. While strain gauges were employed to assess structure deformation and pressure taps were used to evaluate the pressure for the test matrix, displacements were measured by recurring to photogrammetry and laser scan, detecting the position of a set of markers located on the lower wing surface. The inclination of the balance was measured during the runs in order to remove the deformation of the supporting system from the measurements. After the completion of the RIBES project all the data and information relative to this testing campaign were released to the public and are now available for download from the RIBES website (Ribes (2018)).

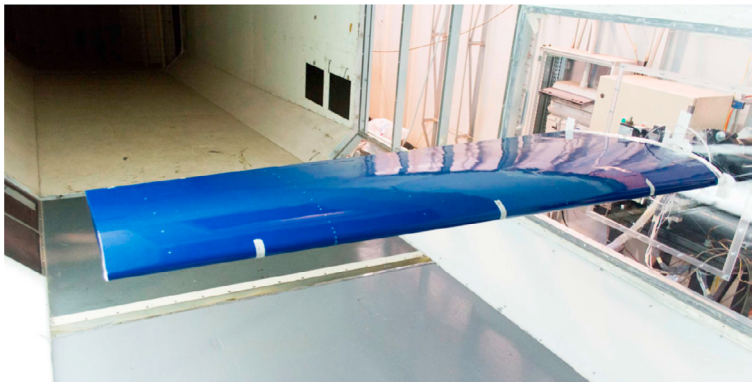

Fig. 5. RIBES wing installation in the wind tunnel

4. Structural validation

The experimental and numerical activities presented in this paper were partially conducted after the completion of the RIBES project; they were not originally scheduled and are part of a subsequent campaign aimed to a specific validation of the numerical structural model employed.

Two different numerical models were developed at increasing level of detail.

The first model, employed for FSI validation and available from the RIBES website, is composed by 97000 shell elements, taking into account the surfaces of the spars, ribs and skins. Ribs caps were not modeled, and the spar caps and stringers were joined to the skin by linking the common nodes in coincidence with the rivets. Upper, lower and leading edge skin panels were joined together following the same strategy. Ribs and trailing edge skin were continuously constrained to the skin.

The material employed was 2024-T3 aluminum alloy, with different properties according to the thickness of each panel.

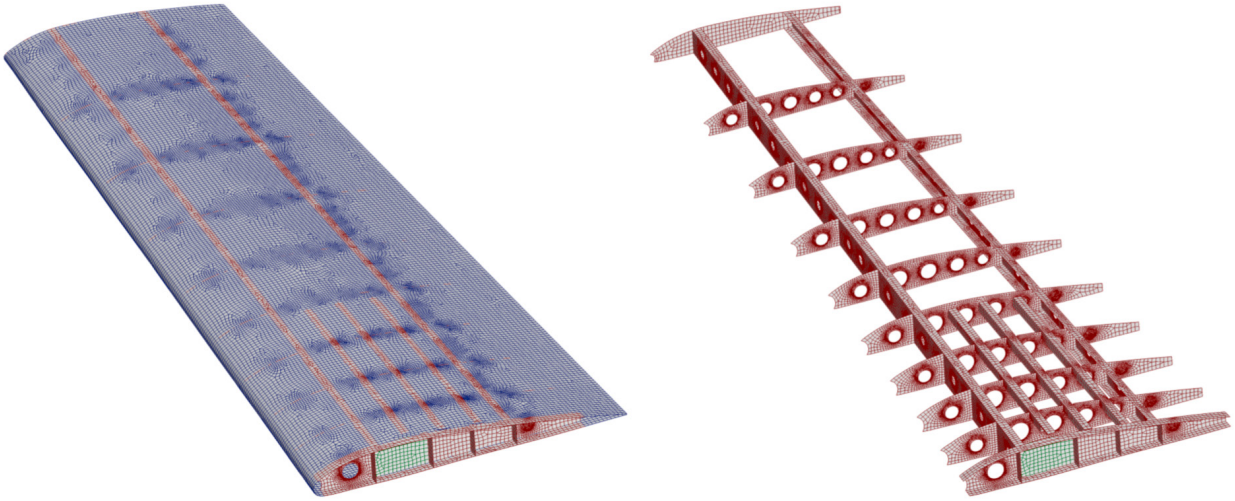

Fig. 6. FEM model of the RIBES wing. Left: assembly, right: spars and ribs

The mass of the numerical model, 4.59 Kg, is way lower than the one of the real RIBES wing, that is 5.8 Kg. This difference is due primarily to the simplifying assumptions that were made, non including several elements such as rivets, linchpins, tubes, wires, sensors, primer and even paint. This dissimilarity, while important in dynamic analyses, has no influence in a static phenomenon and was chosen to be underestimated for this kind of validation.

To validate this structural model the stress values extracted using the strain gauges during one of the runs of the test matrix were employed. Specifically the run with flow speed of 40 m/s and 7 degree of Angle of attack (AoA) was chosen, generating 59.420 Kg of lift load.

Under this boundary condition was carried an FSI analysis and stress values resulting from the static converged solution were compared to the ones obtained in the wind tunnel. Due to a failure to strain gauge number 1 was not possible however to extract the experimental value of stress from this sensor.

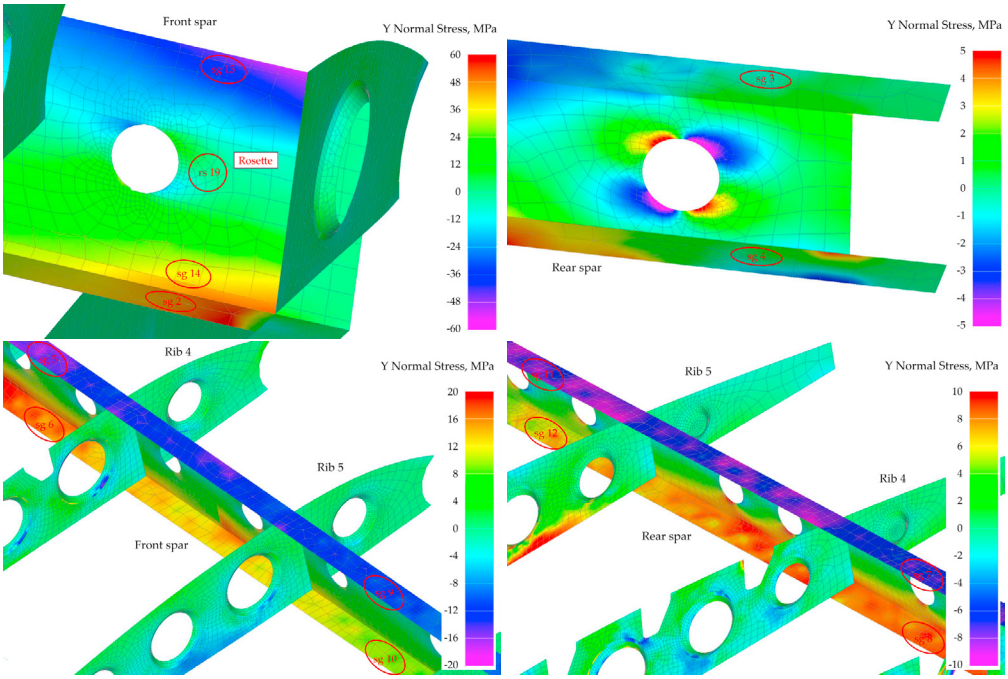

Fig. 7. FEM contours for the first numerical model. Strain gauges are highlighted

In figure 7 the σ_y contours computed using FEM are shown. A reasonable match between experimental and numerical values is achieved and shown in table 2.

Table 2. FEM solution for the first numerical model compared to experimental values

ID	position	measured σ_y (MPa)	FEM σ_y (MPa)
1	front spar	n.a.	~ -47
2	front spar	58.1	~ 46
3	rear spar	-1.2	~ -1
4	rear spar	0.2	~ 2
5	front spar	-17.5	~ -16
6	front spar	18.2	~ 15
7	rear spar	-9.5	~ -7
8	rear spar	11.5	~ 9
9	front spar	-12.2	~ -11
10	front spar	12.3	~ 10
11	rear spar	-8	~ -8
12	rear spar	7.5	~ 6
13	front spar thickening	-15.6	~ -38
14	front spar thickening	15	~ 36
15	upper skin	-143.2	~ -21
17	upper skin	-31.5	~ -15

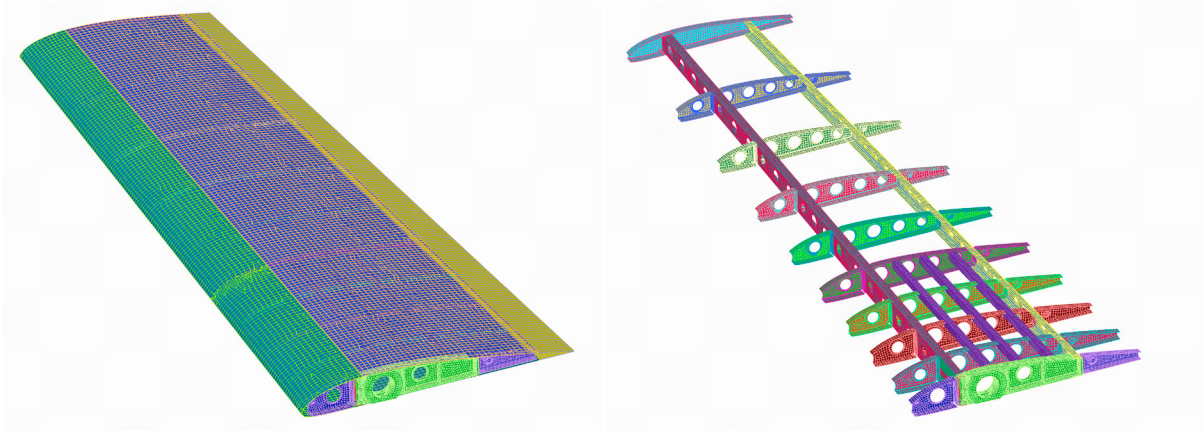

Fig. 8. second FEM model of the RIBES wing. Left: assembly, right: spars, ribs, stringers.

Some discrepancies however are highlighted especially in coincidence of the front spar thickening (strain gauges 13 and 14) and in the junction area between upper skin and root rib (strain gauges 15 and 17). This behavior could be explained by the simplifying assumptions that were made, not modelling the riveted junctions between reinforcements and front spar. Another possible source of uncertainty and discrepancy between experimental and numerical data could be also the connection between front spar and root rib, that are in the RIBES wing linked using two linchpins not modeled in the FEM model. For these reasons a new numerical model was generated including a more refined modeling of the junctions, with the goal of obtaining a more accurate reproduction of stress values. The second numerical model of the RIBES wing, shown in figure 8, is composed by 74389 elements, 50940 of which are linear quad plates employed to model the thin aluminum sheets of the spars, ribs and skins.

The root spar, machined from an aluminum solid, was modeled using solid parabolic tetrahedral elements, in order to obtain an accurate behavior of the root area. Ribs caps were modeled and the fastener flexibility of each rivet was taken into account by employing spring elements. The stiffness of each rivet was calculated using the Huth-Schwarmann (Tate and Rosenfeld (1946)) formula in the form:

$$f = \left(\frac{t_1 + t_2}{2 \cdot d}\right)^a \cdot \frac{b}{n} \cdot \left(\frac{1}{t_1 \cdot E_1} + \frac{1}{n \cdot t_2 \cdot E_2} + \frac{1}{2 \cdot t_1 \cdot E_f} + \frac{1}{2 \cdot n \cdot t_2 \cdot E_f}\right) \tag{1}$$

in which a and b are constants that vary if the junction is a rivet or a bolt and t, E, d are the parameters of each junction in term of plate thickness, Young modulus and hole diameter. To validate this model a static measurement

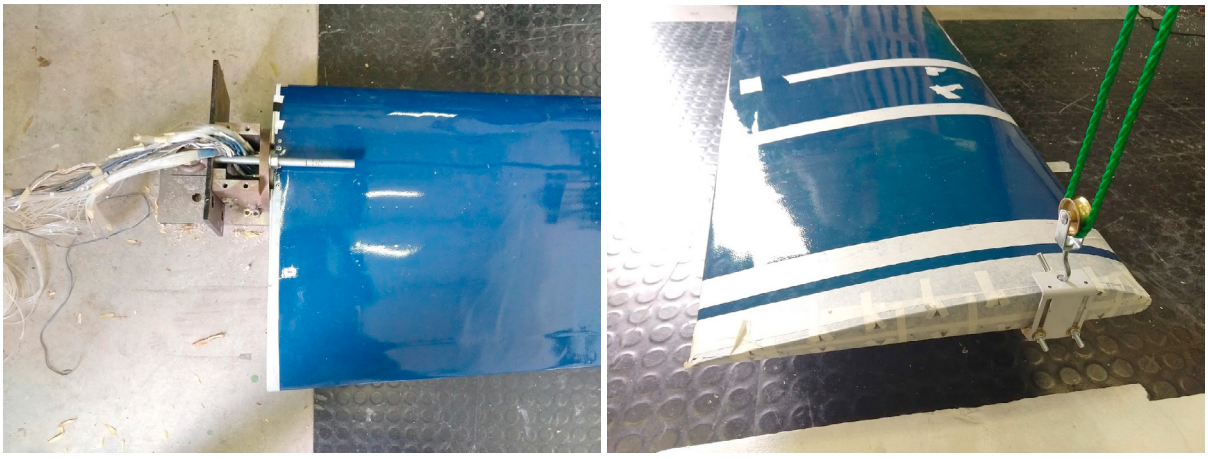

Fig. 9. RIBES wing installation for static loading

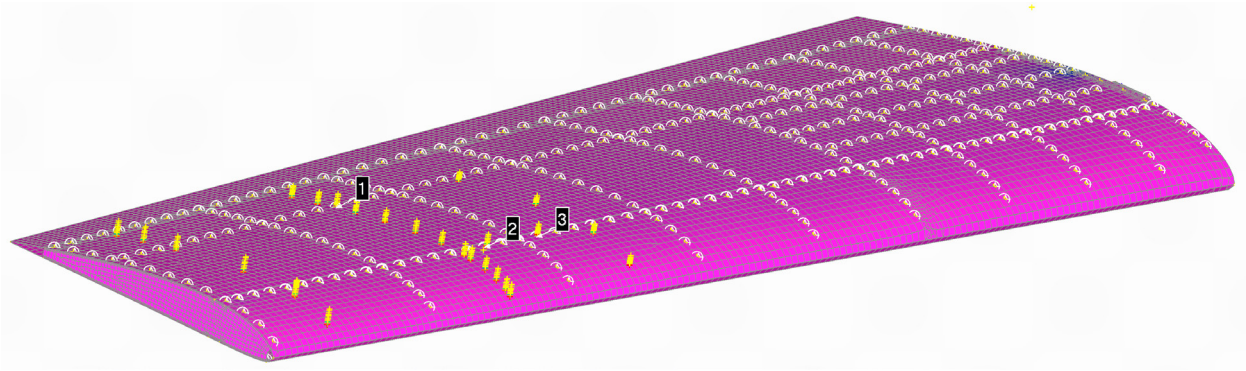

Fig. 10. RIBES Static loading displacements overimposed to the numerical model

campaign was carried at the university of Tor Vergata premises, applying an increasing load to the wing tip from 0 to 7 Kg. Root rib was fixed to the ground to reduce possible measurement errors. In figure 9 the wing mounting and loading clamp are shown. Displacements were measured using a MicroScribe G measuring arm at chosen rivets and in correspondence to the pressure taps at sections 5 and 6. Results were overimposed to the numerical model as shown in figure 10, were the spring elements employed to model the riveted junctions are clearly visible.

Numerical displacements were compared to experimental values for the rivet number 1 shown in figure 10. In figure 11 FEM results show a good agreement with experimental data: the linear analysis follows the trend shown by measured displacements.

This mesh was furtherly tested applying the same boundary conditions employed for the first model, replicating the pressure distribution of the wind tunnel with a 40 m/s flow and 7 degree of AoA. Stresses in correspondence to strain gauges, shown in table 3, exhibit a good match, improving results from the first mesh.

Discrepancies for strain gauges 13, 14, 15 and 17 were reduced but remain consistent especially for the sensors on the upper skin. This area was interested by high stress levels, and during wing assembly phase some of the aluminum rivets were replaced by stronger steel ones. This possibly could led to stress fields that are not accurately reproduced by second numerical model (more accurate one). A more accurate study of the wing structure in this specific location and consequent FEM model refinement are currently scheduled in order to reduce discrepancies and increase the numerical model accuracy.

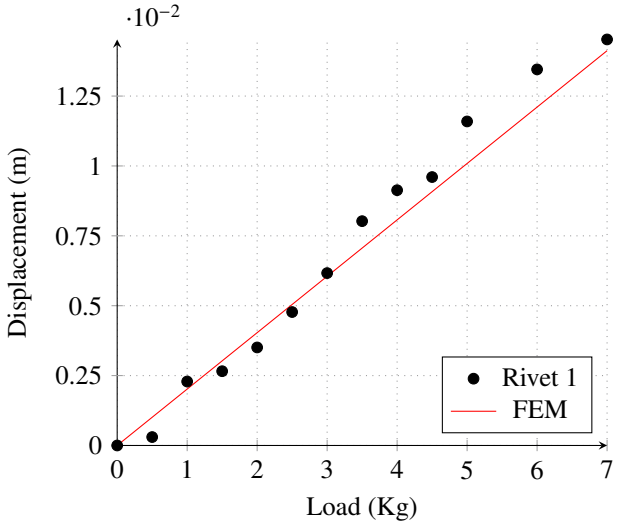

Fig. 11. Experimental vs. FEM displacements for rivet number 1

Table 3. FEM solution for the second numerical model compared to experimental values

ID	position	measured σ_y (MPa)	FEM σ_y (MPa)
2	front spar	58.1	~ 56
3	rear spar	-1.2	~ -1
4	rear spar	0.2	~ 2
5	front spar	-17.5	~ -18
6	front spar	18.2	~ 18
7	rear spar	-9.5	~ -9
8	rear spar	11.5	~ 11
9	front spar	-12.2	~ -11
10	front spar	12.3	~ 11
11	rear spar	-8	~ -8
12	rear spar	7.5	~ 8.9
13	front spar thickening	-15.6	~ -20
14	front spar thickening	15	~ 11
15	upper skin	-143.2	~ -50
17	upper skin	-31.5	~ -20

5. Conclusions

In this paper the design, manufacturing and validation tasks performed on the RIBES test case wing model were reviewed. Two numerical models were developed and validated, comparing results to wind tunnel data but also to static loading. Both models show an acceptable agreement with experimental data and the complexity introduced by rivet modeling and the use of rib caps translated in better results. Discrepancies on the more loaded region of the upper skin however are found for both models, requiring an in depth investigation of the test article. Static testing and validation are the first steps in view of the dynamic characterization of the RIBES test article and of the tuning of the numerical model. This activity, just begun with the University of Rome ”La Sapienza”, will enable a proper modeling of unsteady FSI.

References

Beltramme, D., 2015. Advanced Optimization of the WT Model of the RIBES Project. Master’s thesis. University of Rome ”Tor Vergata”. Rome, Italy.

Biancolini, M., Chiappa, A., Giorgetti, F., Groth, C., Cella, U., Salvini, P., 2018. A balanced load mapping method based on radial basis functions and fuzzy sets. International Journal for Numerical Methods in Engineering 115, 1411–1429. URL: https://onlinelibrary.wiley.com/doi/abs/10.1002/nme.5850, doi:10.1002/nme.5850, arXiv:https://onlinelibrary.wiley.com/doi/pdf/10.1002/nme.5850.

Biancolini, M.E., 2012. Mesh Morphing and Smoothing by Means of Radial Basis Functions (RBF). Handbook of Research on Computational Science and Engineering I, 347–380. doi:10.4018/978-1-61350-116-0.ch015.

Cella, U., 2015. Setup and Validation of High Fidelity Aeroelastic Analysis Methods Based on RBF Mesh Morphing. Ph.d thesis. University of Rome Tor Vergata.

Cella, U., Biancolini, M.E., Groth, C., Chiappa, A., Beltramme, D., 2015. Development and validation of numerical tools for fsi analysis and structural optimization: the eu ribes project status, in: AIAS 44th National Congress, 2 / 5 September 2015, Messina, Italy.

Chen, B.H., Reimer, L., Behr, M., Ballmann, J., 2010. Preinvestigations of a redesigned hirenasd wing model in preparation for new aero-structural dynamic experiments in etw , 411–425.

Chwalowski, P., Florance, J.P., Heeg, J., Wieseman, C.D., Perry, B.P., 2011. Preliminary computational analysis of the (hirenasd) configuration in preparation for the aeroelastic prediction workshop, in: International Forum on Aeroelasticity and Structural Dynamics; 26 / 30 June 2011, Paris, France.

European Commission, 2018. CORDIS website, RIBES project. URL: https://cordis.europa.eu/project/rcn/192637_en.html. last retrieved in date 2018-07-30.

Ribes, 2018. Ribes website. URL: http://ribes-project.eu/. last retrieved in date 2018-07-30.

Tate, M., Rosenfeld, S., 1946. Preliminary investigation of the loads carried by individual bolts in bolted joints. National Advisory Committee for Aeronautics. Technical Report. Technical Note.

Yates, E.C., 1988. AGARD Standard Aeroelastic Configurations for Dynamic Response 1: Wing 445.6, in: The 61st Meeting of the Structures and Materials Panel. URL: http://ntrs.nasa.gov/search.jsp?R=19880017809, doi:10.1049/ip-e.1987.0040.